3D inversion of full tensor magnetic gradiometry (FTMG) data

Michael S. Zhdanov, University of Utah and TechnoImaging, Hongzhu Cai, University of Utah, and Glenn A. Wilson, TechnoImaging*

Summary

Following recent advances in SQUID technology, full tensor magnetic gradiometry (FTMG) is emerging as a practical exploration method. We introduce 3D regularized focusing inversion for FTMG data. Our model studies show that inversion of magnetic tensor data can significantly improve resolution compared to inversion of magnetic vector data for the same model. We present a case study for the 3D inversion of GETMAG® FTMG data acquired over a magnetite skarn at Tallawang, Australia. The results obtained from our 3D inversion agree very well with the known geology of the area.

Introduction

Magnetic vector data measured from orthogonal fluxgate magnetometers are dominated by the earth's background magnetic field, and are thus very sensitive to instrument orientation. Given the relative instabilities of airborne platforms, cesium vapor magnetometers have been preferred, as they directly measure the total magnetic intensity (TMI) and are insensitive to instrument orientation. Total field gradients measured from two (or more) cesium vapor magnetometers are still very sensitive to system orientation and are not "true" potential fields. As such, most magnetic inversion methods are based on TMI data (e.g., Li and Oldenburg, 1996, 2003; Portniaguine and Zhdanov, 2002).

At the same time, as discussed by Schmidt and Clark (2006), direct measurements of magnetic tensors are advantageous for a number of reasons. First, magnetic tensors are relatively insensitive to instrument orientation since magnetic gradients arise largely from localized sources and not the Earth's background field or regional trends. Second, magnetic tensor data obviates the need for base stations and diurnal corrections. Third, magnetic tensor data contain directional sensitivity, which is advantageous for the interpretation of under-sampled surveys. And finally, remanent magnetization, including the Koenigsberger ratio, can be recovered from magnetic tensor data.

Recently, full tensor magnetic gradiometers based on superconducting quantum interference devices (SQUIDs) have been developed and are now being commercially deployed for geophysical surveying (e.g., Schmidt et al., 2004; Stolz et al., 2006; Rompel, 2009). Given the prior applications of magnetic gradiometry, which have been used for the real-time tracking of objects from stationary or moving platforms, magnetic tensor data has been usually interpreted by some type of Euler deconvolution (e.g., Wynn et al., 1975). While these methods may provide information about the sources, it is not immediately obvious how that information can be related to the quantitative analysis of a 3D susceptibility model for subsurface characterization.

We present 3D inversion of full tensor magnetic gradiometry (FTMG) data using the principles of the regularized focusing inversion (Zhdanov, 2002). We demonstrate our software with model studies, and a case study for 3D inversion of GETMAG® magnetic tensor data acquired over a magnetite skarn at Tallawang, Australia. In particular, we demonstrate how focusing regularization recovers a susceptibility model that better corresponds to the known geology than the model recovered with smooth regularization.

Inversion methodology

In what follows, we adopt the common assumption that there is no remanent magnetization, that the self-demagnetization effect is negligible, and that the magnetic susceptibility is isotropic. Under such assumption, the intensity of magnetization is linearly related to an inducing magnetic field through the magnetic susceptibility:

$$I(\mathbf{r}) = \chi(\mathbf{r})H^0(\mathbf{r}).$$

We discretize the 3D earth model into a grid of N_m cells, each of constant magnetic susceptibility. Following Zhdanov (2002), the magnetic potential can be expressed in discrete form as follows:

$$U(\mathbf{r}') = \sum_{k=1}^{N_m} \chi_k \iiint_{D_k} \psi(\mathbf{r}', \mathbf{r}) dv,$$

where $\psi(\mathbf{r}', \mathbf{r})$ is the whole-space Green's function for the magnetic potential. All magnetic fields can be computed as spatial derivatives of the above equation. For example, the magnetic field vectors are the first spatial derivatives of the magnetic potential:

$$H_\alpha(\mathbf{r}) = \frac{\partial U(\mathbf{r})}{\partial \alpha}, \alpha = x, y, z.$$

The second spatial derivatives of the magnetic potential,

$$H_{\alpha\beta}(\mathbf{r}) = \frac{\partial U(\mathbf{r})}{\partial\alpha\partial\beta}, \alpha, \beta = x, y, z,$$

form a symmetric tensor with zero trace:

$$\hat{\mathbf{H}}(\mathbf{r}) = \begin{bmatrix} H_{xx} & H_{xy} & H_{xz} \\ H_{yx} & H_{yy} & H_{yz} \\ H_{zx} & H_{zy} & H_{zz} \end{bmatrix}.$$

Our regularized inversion is based on the regularized re-weighted conjugate gradient (RRCG) method with options for smooth or focusing regularization. We can either jointly or independently invert all components of the magnetic vectors and/or tensors. Positivity of the susceptibility is enforced. All data and model weights are based upon their integrated sensitivity (Zhdanov, 2002). Our weighting functions provide equal sensitivity of the different components of observed data to cells located at different depths and horizontal positions. Thus, our weighting functions automatically introduce appropriate corrections for the vertical and horizontal distribution of the susceptibility. This is one of the main differences between our approach, and the variety of geometric weighting functions commonly used by others.

Model study

To investigate the performance of our 3D inversion for both magnetic vector and tensor data, we considered two synthetic 3D models. In both cases, the magnetic vector data consisted of three vector components, and the magnetic tensor data consisted of all five independent tensor components. All inversion results were obtained using focusing (minimum support) regularization.

The first synthetic model consists of a rectangular body 60 m wide with a 10 m × 10 m of cross-sectional area, buried 30 m below the surface. The susceptibility of the body is 1, and it is embedded in an otherwise homogeneous and nonmagnetic host. The inducing magnetic field has an inclination of 90 degrees and a declination of zero degrees. Since we wanted to compare the inversion results for both magnetic vector and tensor data, we did not contaminate either data with noise. The results are shown in Figure 1. As can be seen, the body is recovered from both vector and tensor inversions; as expected, the latter provides a more compact image of the body.

The second synthetic model consists of two rectangular bodies. The first body is 60 m wide, with a 10 m × 10 m cross-sectional area, and is buried 30 m below the surface. The second body is separated by 90 m from the first body, is 40 m wide, with a 10 m × 10 m cross-sectional area, and is buried 30 m below the surface as well. The susceptibility of both bodies is 1, and they are embedded in an otherwise homogeneous and nonmagnetic host. The inducing magnetic field has an inclination of 90 degrees and a declination of zero degrees. Since we wanted to compare the inversion results for both magnetic vector and tensor data, we did not contaminate either data with noise. The results are shown in Figure 2. As can be seen, the bodies were recovered from both vector and tensor inversions; as expected, the latter provides a more compact image of the bodies.

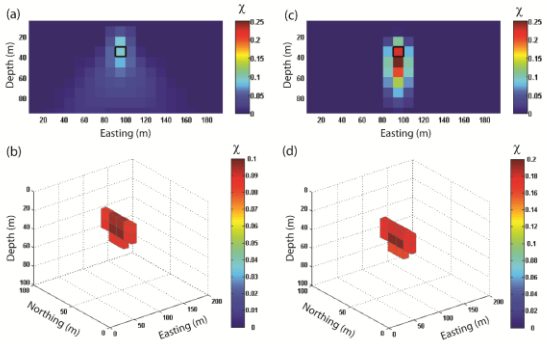

Figure 1. *3D inversion results for magnetic vector data over a single block: (a) vertical cross section along 50 m northing, and (b) 3D perspective with a 0.1 cut-off applied to the susceptibility distribution. 3D inversion results for magnetic tensor data over a single block: (c) vertical cross section along 50 m northing, and (d) 3D perspective with a 0.2 cut-off applied to the susceptibility distribution.*

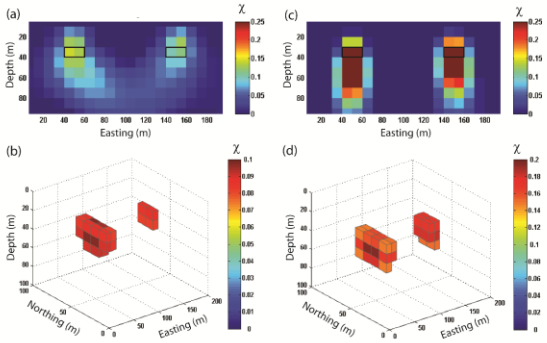

Figure 2. *3D inversion results for magnetic vector data over two blocks: (a) vertical cross section along 50 m northing, and (b) 3D perspective with a 0.1 cut-off applied to the susceptibility distribution. 3D inversion results for magnetic tensor data over two blocks: (c) vertical cross section along 50 m northing, and (d) 3D perspective with a 0.2 cut-off applied to the susceptibility distribution.*

Case study – 3D inversion of GETMAG® data from Tallawang, New South Wales, Australia

The most appropriate sensors for measuring magnetic tensors are superconducting quantum interference devices (SQUIDs), which detect minute changes of flux threading a superconducting loop. They are therefore variometers rather than magnetometers, but they are vector sensors since only changes perpendicular to the loop are detected (Foley and Leslie, 1998; Foley et al., 1999; Lee et al., 2001). High-temperature superconducting (HTS) SQUIDs operate at liquid nitrogen temperatures (77 K), overcoming operational difficulties related to the handling of liquid helium (4 K) as required for low-temperature superconducting (LTS) SQUIDs.

Based on Tilbrook (2004), CSIRO's GETMAG® magnetic gradiometer (Schmidt et al., 2004) is an integrated package of three rotating single-axial gradiometer sensors in an umbrella arrangement, as shown in Figure 3. This configuration has several distinct advantages. First, it reduces the required number of sensors and electronics. Second, the amount of cross-talk between sensors is reduced by employing different rotation frequencies. This shifts the measurement (rotation) frequency from quasi-DC to tens or hundreds of hertz, leading to a reduced intrinsic sensor noise and a reduced influence of low-frequency mechanical vibrations; thus the requirements for a suspension system for airborne deployment are significantly reduced. Third, by implementing data extraction through Fourier analysis, magnetic vectors can be separated from magnetic tensors as the signals are centered at the fundamental frequency and at twice the rotation frequency, respectively. Thus, with only three single-axial sensors, all vector and tensor components can be recovered.

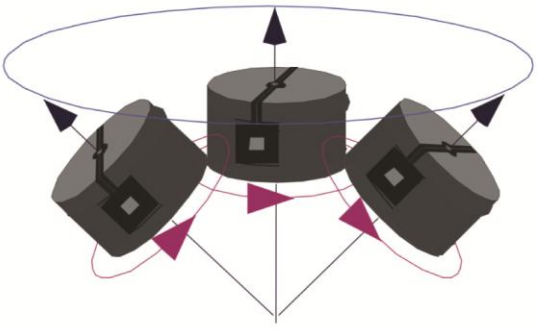

Figure 3. *Schematic diagram of CSIRO's GETMAG® sensor configuration with the three rotating SQUID sensors in an umbrella configuration (from Schmidt et al., 2004).*

Schmidt et al. (2004) demonstrated CSIRO's GETMAG system with a field trial of three profiles (50 mN, 60 mN, and 120 mN) over a magnetite skarn deposit at Tallawang, near Gulgong in New South Wales, Australia (Figure 4). The deposit is roughly tabular, striking NNW and dipping steeply to the west. The survey was approximately perpendicular to strike, minimizing aliasing and effectively making the surveys 2D. The Tallawang magnetite skarn is located along the western margin of the Gulgong Granite, which was intruded during the Kanimblan Orogeny in the Late Carboniferous. In detail, the magnetite occurs in lenses thought to reflect replacement of a tightly folded host rock sequence (Tucklan Beds), and is additionally complicated by transverse faulting, causing east-west displacement of the magnetite zones. The magnetite body is well delineated by numerous drill holes, and the magnetic rock properties of the magnetite have been well characterized. The strongest samples possessed susceptibility of 3.8 SI (0.3 cgs) and remanence of 40 Am^{-1}, yielding Köenigsberger ratios (Qs) between 0.2 and 0.5. The mean direction of the remanence is WNW and steeply up. This direction may be the result of a dominant viscous remanent magnetization (VRM) in the direction of the recent geomagnetic field, and a reversed mid-Carboniferous component, dating from the time that the Gulgong Granite was intruded. The effective magnetization, projected onto a vertical plane perpendicular to strike, is directed steeply upward.

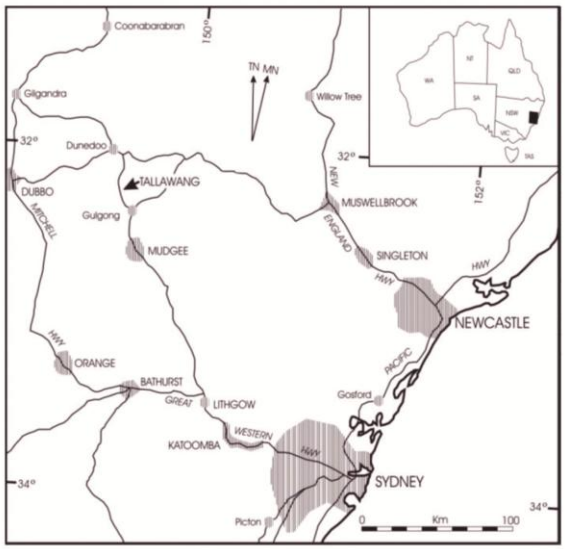

Figure 4. *Location of the Tallawang magnetite skarn in New South Wales, Australia (from Schmidt et al., 2004).*

We applied our 3D inversion to the three profiles of the GETMAG® data to obtain 3D susceptibility images. First, we inverted the data using minimum support (focusing) regularization. For comparison, we then inverted the data using minimum norm (smooth) regularization. Both inversions terminated at a common misfit of 10%. Figures 5a to 5d show vertical and horizontal cross sections beneath each of the profiles and at 25 m depth as obtained from 3D inversion with focusing regularization. Figures 5e to 5h show vertical and horizontal cross sections beneath each of the profiles and at 25 m depth as obtained from 3D inversion with smooth regularization. Both models satisfy the data to the same misfit, yet we can clearly see how focusing regularizations enables us to recover much sharper boundaries and higher contrasts than smooth regularization. Moreover, as we superimposed the geology (Figure 6), we can see excellent agreement between our focusing inversion results and the known geology where we have sensitivity.

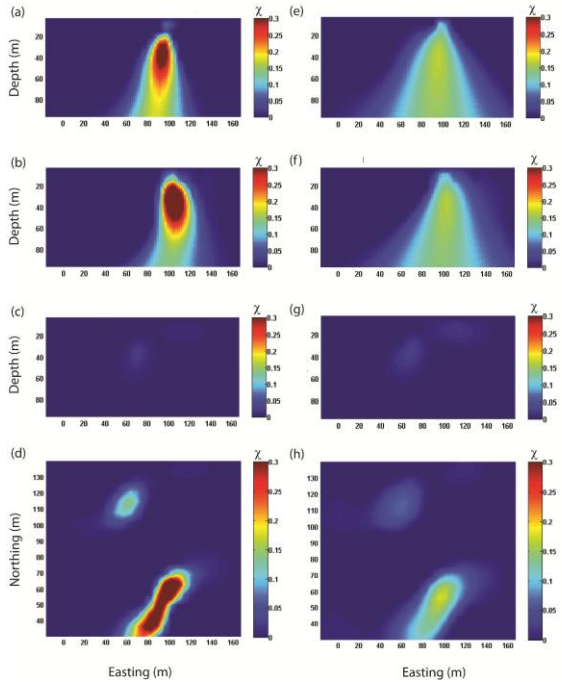

Figure 5. *Results of 3D inversion with minimum support (focusing) regularization for vertical cross sections along profiles (a) 50 mN, (b) 60 mN, and (c) 120 mN; and (d) horizontal cross section at 25 m depth. For comparison, results are also shown for 3D inversion with minimum norm (smooth) regularization for vertical cross sections along profiles (e) 50 mN, (f) 60 mN, and (g) 120 mN; and (h) horizontal cross section at 25 m depth.*

Conclusions

We have developed 3D regularized inversion for full tensor magnetic gradiometry (FTMG) data. Our model studies have shown that inversion of all independent magnetic tensor components can significantly improve model resolution compared to inversion of magnetic vector components. In practice, inversion of all magnetic tensor components effectively increases the signal-to-noise ratio. We have applied our 3D inversion to GETMAG® magnetic tensor data acquired over a magnetite skarn at Tallawang in New South Wales, Australia. Our results agree very well with the known geology of the area, and show how FTMG can significantly improve the practical effectiveness of magnetic methods for exploration.

Acknowledgements

The authors acknowledge TechnoImaging for support of this research. Zhdanov and Cai acknowledge support of the University of Utah's Consortium for Electromagnetic Modeling and Inversion (CEMI). The authors thank CSIRO Materials Science and Engineering, in particular Phillip Schmidt, David Clark, Keith Leslie, and Cathy Foley, for providing the Tallawang GEMTAG® data and related material.

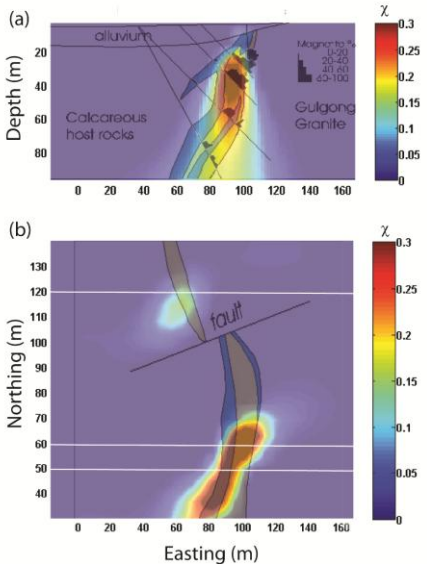

Figure 6. *Geology of the Tallawang magnetite skarn superimposed on the susceptibility model recovered from 3D inversion of GETMAG data using minimum support (focusing) regularization for (a) vertical cross section along profile 50 mN, and (b) horizontal cross section at 25 m depth.*

EDITED REFERENCES

Note: This reference list is a copy-edited version of the reference list submitted by the author. Reference lists for the 2011 SEG Technical Program Expanded Abstracts have been copy edited so that references provided with the online metadata for each paper will achieve a high degree of linking to cited sources that appear on the Web.

REFERENCES

Foley, C. P., and K. E. Leslie, 1998, Potential use of High Tc SQUIDS for airborne electromagnetics: Exploration Geophysics, **29**, 30–34, doi:10.1071/EG998030.

Foley, C. P., K. E. Leslie, R. Binks, C. Lewis, W. Murray, G. J. Sloggett, S. Lam, B. Sankrithyan, N. Savvides, A. Katzaros, K.-H. Muller, E. E. Mitchell, J. Pollock, J. Lee, D. L. Dart, R. R. Barrow, M. Asten, A. Maddever, G. Panjkovic, M. Downey, C. Hoffman, and R. Turner, 1999, Field trials using HTS SQUID magnetometers for ground-based and airborne geophysical applications: IEEE Transactions on Applied Superconductivity, **9**, 3786–3792, doi:10.1109/77.783852.

Lee, J. B., R. J. Turner, M. A. Downey, A. Maddever, D. L. Dart, C. P. Foley, R. Binks, C. Lewis, W. Murray, G. Panjkovic, and M. Asten, 2001, Experience with SQUID magnetometers in airborne TEM surveying: Exploration Geophysics, **32**, 9–13, doi:10.1071/EG01009.

Li, Y., and D. W. Oldenburg, 1996, 3-D inversion of magnetic data: Geophysics, **61**, 394–408, doi:10.1190/1.1443968.

Li, Y., and D. W. Oldenburg, 2003, Fast inversion of large-scale magnetic data using wavelet transforms and a logarithmic barrier method: Geophysical Journal International, **152**, 251–265, doi:10.1046/j.1365-246X.2003.01766.x.

Portniaguine, O., and M. S. Zhdanov, 2002, 3-D magnetic inversion with data compression and image focusing: Geophysics, **67**, 1532–1541, doi:10.1190/1.1512749.

Rompel, A. K. K., 2009, Geologic applications for FTMG: Presented at 11th SAGA Biennial Technical Meeting and Exhibition, 39–42.

Schmidt, P., D. Clark, K. Leslie, M. Bick, D. Tilbrook, and C. Foley, 2004, GETMAG – a SQUID magnetic tensor gradiometer for mineral and oil exploration: Exploration Geophysics, **35**, 297–305, doi:10.1071/EG04297.

Schmidt, P. W., and D. A. Clark, 2006, The magnetic gradient tensor: Its properties and uses in source characterization: The Leading Edge, **25**, 75–78, doi:10.1190/1.2164759.

Stolz, R., V. Zakosarenko, M. Schulz, A. Chwala, L. Fritzsch, H.-G. Meyer, and E. O. Köstlin, 2006, Magnetic full-tensor SQUID gradiometer system for geophysical applications: The Leading Edge, **25**, 178–180, doi:10.1190/1.2172308.

Tilbrook, D. L., 2004, The design of a new concept HTSC axial gradiometer: Physica C, Superconductivity, **407**, 1–9, doi:10.1016/j.physc.2004.04.025.

Wynn, W., C. Frahm, P. Carroll, R. Clark, J. Wellhoner, and M. Wynn, 1975, Advanced superconducting gradiometer/Magnetometer arrays and a novel signal processing technique: IEEE Transactions on Magnetics, **11**, 701–707, doi:10.1109/TMAG.1975.1058672.

Zhdanov, M. S., 2002, Geophysical inverse theory and regularization problems: Elsevier.